228 (2023) 212045

Contents lists available at ScienceDirect

Geoenergy Science and Engineering

journal homepage: www.sciencedirect.com/journal/geoenergy-science-and-engineering

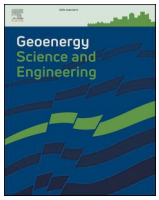

A multiphysics model for biogenic gas extraction from coal seams

Qi Gao [a], Jishan Liu [a,*], Yaoyao Zhao [b], Mingyao Wei [c], Yee-Kwong Leong [a], Derek Elsworth [d]

[a] School of Engineering, The University of Western Australia, Perth, WA 6009, Australia
[b] State Key Laboratory of Coal Resources & Safe Mining, China University of Mining & Technology, Beijing 100083, China
[c] National and Local Joint Engineering Laboratory of Internet Application Technology on Mine, IoT Perception Mine Research Center, China University of Mining and Technology, Xuzhou, Jiangsu 221116, China
[d] Department of Energy and Mineral Engineering, G3 Centre and Energy Institute, The Pennsylvania State University, University Park, PA 16802, USA

ARTICLE INFO

Keywords:
Biogenic methane
Coal bioconversion
Multiphysics model
Microbially enhanced coalbed methane

ABSTRACT

Approximately 20% of global natural gas resources, including coalbed methane (CBM), could be microbial in origin. This discovery has attracted great interests in extracting biogenic gas in coal seams. Previous studies have demonstrated that this could be achieved through injecting nutrients solution, either with or without microbes, into a coal reservoir. The injected nutrients transport in coal, stimulate the growth of microbes, and enhance their metabolic activities. Through these complex processes, the organic components in coal are biodegraded into methane gas. The generated biogenic gas may be either in free phase or adsorbed on coal grains and can be extracted as an integral part of the gas-in-place. Although this bio-stimulation technique has been proposed for decades, generating and extracting additional biogenic methane in coal seams is still in a stage of conceptual development. In this study, we develop a modelling tool to validate this concept under the laboratory conditions and upscale to reservoir conditions. The model consists of a complete set of partial differential equations (PDEs) to define: (1) coal deformation, (2) water and gas flow, (3) multispecies reactive transport, and (4) microbial growth/decay and adsorption/desorption. All these processes are coupled through coal porosity and permeability model that links hydrological, mechanical, chemical and biological processes together. The multiphysics model is verified against laboratory coal bioconversion data. The verified model is applied to simulate practical operation in which nutrients solution is continuously delivered into coal seams. Simulation results capture all important processes involved and validate the effectiveness of coal-to-methane bioconversion and its extraction.

1. Introduction

CBM is a typical type of unconventional natural gas resources with origins being either thermogenic or biogenic (Park and Liang, 2016). Thermogenic CBM is generated through devolatilization of coal under the high pressure and high temperature conditions during the coalification process, while biogenic CBM is generated through microbial degradation of organic components in coal over time (Lupton et al., 2020). Studies have suggested that around 20% of the global natural gas resources, including CBM, could be microbial in origin (Rice and Claypool, 1981). This implies the great potential of applying bio-stimulation technique to enhance CBM recovery. In 1995, Scott (1995) first introduced the concept of microbially enhanced coalbed methane (MECBM) which aims to replicate the natural generation process of biogenic methane by treating coal with microbes and suitable nutrients solution. Under the nutrient-rich condition, the growth and metabolic activities of microbes are promoted and then biogenic methane is gradually generated through microbial degradation of coal.

Bioconversion of coal to methane is a reverse process of CBM extraction (Pandey et al., 2016). During CBM extraction, three serial processes occur in coal seams including gas desorption from coal grains, gas diffusion out of coal matrix and then gas flow in the fractures. By contrast, these processes are reversed during coal bioconversion. First, methane gas is generated and flows in the fracture system. Then, a portion of gas diffuses into coal matrix under the pressure difference between fracture and matrix systems. Finally, this portion of gas adsorbs on coal grains with the increasing pressure. Therefore, coal bioconversion is able to extend the lifespan of depleted CBM reservoirs.

In recent years, research in the area of coal bioconversion has accelerated. Many experiments have been conducted from the microbial treatment perspective. These experimental efforts spanned from understanding coal bioconversion pathways (Strapoc et al., 2008, 2011) to improving biogenic methane generation through using different

* Corresponding author.
E-mail address: jishan.liu@uwa.edu.au (J. Liu).

https://doi.org/10.1016/j.geoen.2023.212045
Received 27 May 2022; Received in revised form 26 March 2023; Accepted 30 May 2023
Available online 26 June 2023

Nomenclature

a	Shape factor
c_f	Fracture compressibility
C_n, C_m, C_p	Concentrations of nutrients, microbes and metabolic products
D_n, D_m, D_p	Dispersion coefficients of nutrients, microbes and metabolic products
d_1	Microbial decay rate
E	Elastic modulus
f	Strain splitting factor
f_i	Body force component
g_1	Microbial growth rate
G	Shear modulus
h_0	Initial fracture aperture
h_r	Residual fracture aperture
k_1, k_3, k_2	Reversible adsorption, irreversible adsorption, and desorption rates
k_f, k_m	Fracture and matrix permeabilities
k_{rw}, k_{rg}	Water and gas relative permeabilities
k_{se}	Stress erosion rate
K	Bulk modulus
$K_{m/s}$	Half-saturation constant for microbial growth
p_c	Capillary pressure
p_e	Entry pressure of non-wetting phase
p_f, p_m, p_b	Fracture, matrix and bulk pressures
p_{fw}, p_{fg}	Water and gas pressures in fracture
p_L	Langmuir pressure constant
Q_w, Q_g	Source terms for water and gas
Q_{fm}	Gas mass transfer from fracture to matrix
R_c	Contact area ratio
R_n, R_m, R_p	Reaction source terms of nutrients, microbes and metabolic products
S	Specific surface area
S_w, S_g	Water and gas saturations
S_w^*, S_g^*	Effective saturations of water and gas phases
S_{wi}	Irreducible water saturation
S_{gr}	Residual gas saturation
u_i	Displacement component
v_{fw}	Water flow velocity in fracture
V_{bg}	Biogenic CBM volume generated per unit mass of coal
V_f, V_s, V_b	Fracture, solid and bulk volumes
Y_s	Nutrients consumption rate
α, β, γ	Biot coefficients
δ_{ij}	Kronecker delta
ε_{ij}	Strain tensor component
ε_L	Langmuir strain constant
ε_s	Gas sorption strain
ε_{se}	Stress erosion induced strain
ε_v	Volumetric strain
λ	Pore size distribution coefficient
μ_p	Metabolic product generation rate
μ_w, μ_g	Water and gas viscosities
ρ_c	Coal density
ρ_{ga}	Methane density at standard conditions
ρ_m	Microbial density
ρ_w	Water density
$\overline{\sigma}$	Mean compressive stress
σ_a	Effective stress at contacting asperities
σ_c	Critical stress when stress erosion ceases
σ_{cp}	Confining pressure
σ_{ij}	Stress tensor component
$\varnothing_1$, $\varnothing_2$	Volumetric fractions of microbes adsorbed reversibly and irreversibly on fracture surface
$\varnothing_{mc}$	Total volumetric fractions of microbes adsorbed on fracture surface
$\varnothing_f$	Fracture porosity
$\varnothing_s$	Fraction of coal that has been degraded
$\varnothing_{ns}$	Fraction of coal that cannot be degraded

Abbreviations

CBM	Coalbed methane
MECBM	Microbially enhanced coalbed methane
PDEs	Partial differential equations

microbial communities (Jones et al., 2010; Opara et al., 2012; Gupta and Gupta, 2014), different nutrients solutions (Zhang et al., 2016a), and different testing conditions (Zhang et al., 2016b). It has been found that biogenic methane generation is influenced by many factors including coal rank, coal loading, particle size, temperature, Eh, medium pH, salinity and etc. As these studies were conducted under near ambient pressure and temperature conditions, biogenic methane generation potential under the reservoir conditions remains to be investigated. To this end, Stephen et al. (2014) conducted the core flooding experiment using crushed coal from Highvale mine in Alberta to generate biogenic methane under different pressures from 1720 to 3450 kPa. Meslé et al. (2016) observed biogenic methane generation using crushed coal from Powder River Basin under both 550 kPa and ambient pressure conditions in a pressurized flow column. Saurabh and Harpalani (2018) used crushed coal from Illinois basin to complete the biogenic methane generation experiment under a constant pore pressure of 3 MPa and a constant temperature of 32 °C. An important question still not addressed is that whether biogenic methane generation rate measured using crushed coal can represent that using intact coal. Further, Pandey and Harpalani (2019a) performed bioconversion experiment using intact coal from Illinois basin under the constant confining pressure condition. Lupton et al. (2020) stimulated biogenic methane generation on intact coal from Surat and Bowen Basins under the constant effective stress condition. These experimental results show that biogenic methane can indeed be generated under the reservoir conditions but the gas generation rate of intact coal is much lower than that of crushed coal.

Given that coal seams serve as the source and reservoir rock for generated biogenic methane, it is also important to characterize the changes in gas sorption, fluid flow and geomechanical properties of coal due to bio-treatment. The accurate characterization of these properties helps to assess the reservoir performance during biogenic methane extraction. Zhang et al. (2017) and Pandey et al. (2016) examined the change in gas sorption capacity of coal caused by bioconversion and they found that methane adsorption capacity increases after bio-treatment, while Su et al. (2022) reported the opposite finding. Stephen et al. (2014), Pandey and Harpalani (2019a) and Lupton et al. (2020) conducted core flooding tests to investigate coal permeability change during bio-treatment. Their findings show that coal permeability significantly decreases during nutrients solution injection. In addition, Pandey and Harpalani (2019a, 2019b) also measured the variation of coal cleat compressibility before and after bio-treatment. The results show the increase of cleat compressibility after bioconversion.

Although laboratory experiments are the most direct way to study coal bioconversion process, it is sometimes expensive, time-consuming, and even requires massive manpower. Therefore, theoretical approaches turn to be vital for us to study the problem. Saurabh and Harpalani (2018) developed an analytical model to predict biogenic methane generation under the assumption that methane generation rate is

directly proportional to the population of methanogens. Senthamaraikkannan et al. (2016a), Sharma et al. (2018) and Emmert et al. (2020) proposed numerical solutions to model biogenic methane generation considering the reaction kinetics of coal bioconversion. These numerical models can be applied to predict methane generation under the static condition in the laboratory anaerobic reactors, as opposed to the dynamic flow condition in subsurface coal seams. Senthamaraikkannan et al. (2016b, 2016c) proposed a dual porosity model incorporating the reaction kinetics of coal bioconversion to simulate biogenic methane generation and transport in CBM reservoirs. Only hydrological field is considered in their models. Further, Zhi et al. (2018) developed a coupled hydro-mechanical-chemical model to simulate hydraulic fracturing process for improved nutrients delivery in coal seams but the microbial activities are ignored.

From the above literature review, it can be known that massive research works have been done in the area of coal-to-methane bioconversion with mainly focus on three aspects: enhancing biogenic methane generation from the microbial treatment perspective; measuring the changes in coal physical and mechanical properties due to biotreatment; and mathematical modelling of biogenic methane generation. However, works on modelling the interactions of multiple processes during coal bioconversion are still not available. This limits our understanding of complex processes involved. In this work, we develop a multiphysics model to quantify all the processes involved. In the following, the conceptual model of coal-to-methane bioconversion in coal seams is first introduced. Then, a complete set of PDEs are developed to define the involved processes with all these processes linked through a coal porosity and permeability model. After that, the multiphysics model is verified against laboratory coal bioconversion data. Finally, the verified model is applied to analyze all important processes during coal bioconversion. It should be noted here that CO_2 and H_2 can also be generated during coal bioconversion processes but the focus of this work is on the generation of methane gas. Thus, the word "gas" in this paper refers in particular to biogenic methane.

2. The conceptual model

Microbial stimulation is the primary approach of current commercial MECBM projects. It works through injecting nutrients solution into coal seams to stimulate the growth and metabolic activities of microbes so as to degrade solid coal into methane gas. During microbial stimulation process, nutrients are injected into coal seams using produced formation water in a recirculation process, thereby having the minimum net water removal from the underground formation. The produced formation water usually contains a low concentration of indigenous microbes (Ritter et al., 2015).

When nutrients solution is injected into coal seams, the water-based fluid flows in the fracture system as micropores in coal matrix are inaccessible to water owing to their small pore dimensions (King et al., 1986). In addition, microbes are assumed to be present in the water phase and mainly live within the fracture network. This is because coal matrix pores (typically less than 50 nm in diameter) are usually too small for microbes (typically 1–3 μm) to inhabit (Scott, 1999). Thus, organic components of coal on the fracture surface are gradually degraded by microbes. The microbial degradation of coal to methane gas is a multi-step process which involves the activities of a consortium of microbes. In general, the whole process of coal degradation consists of four steps (Park and Liang, 2016): (1) hydrolysis; (2) acidogenesis; (3) acetogenesis; and (4) methanogenesis. In the first step, the complex organic components in coal are degraded into water-soluble intermediates. In the second step, the water-soluble intermediates are further degraded into simpler compounds. In the third step, the products of acidogenesis are degraded into smaller acids such as acetate, CO_2 and H_2. In the last step, the substrates such as acetate, CO_2 and H_2 are utilized by methanogens to produce biogenic methane. Therefore, water-gas two-phase flow presents in the fracture system during coal bioconversion, along with the dissolved nutrients, microbes and metabolic products in the water phase, as shown in Fig. 1. Note that the metabolic products here only refer to those water-soluble intermediates excluding the generated gases. As the fluid injection pressure is larger than the initial pressure in coal, a pressure difference is created between fracture and matrix systems. This pressure difference increases with the generation of biogenic methane in fracture. Under the pressure difference, a portion of biogenic methane diffuses into coal matrix and adsorbs on coal grains.

Overall, MECBM operation involves the interactions of multiple processes within coal seams. These processes mainly include coal deformation, water and gas flow, multispecies reactive transport, and microbial growth/decay and adsorption/desorption. All these processes can be linked together through a coal porosity and permeability model. During bioconversion, coal porosity and permeability are mainly influenced by the following factors:

(1) Nutrients injection: When nutrients solution is injected into coal seams, pressure in the fracture system increases, effective stress on fracture surface declines and thus coal permeability increases.
(2) Stress erosion: Coal fracture can be idealized as two rough surfaces held apart by contacting asperities. Due to the small contacting area, the local stress at the contacting asperities is greatly enhanced when compressive stress is applied to coal. The stress concentration induces grain-contact crushing, followed by the gradual fracture compaction and coal permeability decline. This slow process is defined as stress erosion. As fracture aperture decreased, the contacting area increases and the local stress decreases concomitantly. Stress erosion and the associated coal permeability decline ceases when local stress approaches the critical stress that implies equilibrium.
(3) Coal solubilization: Under the nutrient-rich condition, the growth and metabolic activities of microbes are stimulated. Then, complex organic components on the fracture surface are gradually biodegraded which leads to fracture aperture and coal permeability increase.
(4) Biogenic methane adsorption: Bioconversion of coal generates biogenic methane. Instead of being extracted, part of the generated biogenic methane diffuses into coal matrix and adsorbs on coal grains which induces coal swelling and results in coal permeability decline.
(5) Microbial adsorption: These microbes adsorbed on the fracture surface occupy a fraction of coal porosity and lead to coal permeability reduction.

Post bio-treatment, whether the ultimate coal permeability is greater or less than the initial coal permeability depends on the net influence of these opposing mechanisms.

3. Governing equations for the coupled processes

MECBM operation involves the injection of nutrients solution into coal seams to stimulate the growth and metabolic activities of microbes so as to degrade solid coal to methane gas (Ritter et al., 2015; Park and Liang, 2016). In this process, complex interactions among coal, nutrients solution, and microbes occur. These interactions exert strong influences on coal deformation, water and gas flow, multispecies reactive transport, microbial growth/decay and adsorption/desorption, and coal porosity and permeability change. In this work, we define coal bioconversion as the coupled hydrological-mechanical-chemical-biological

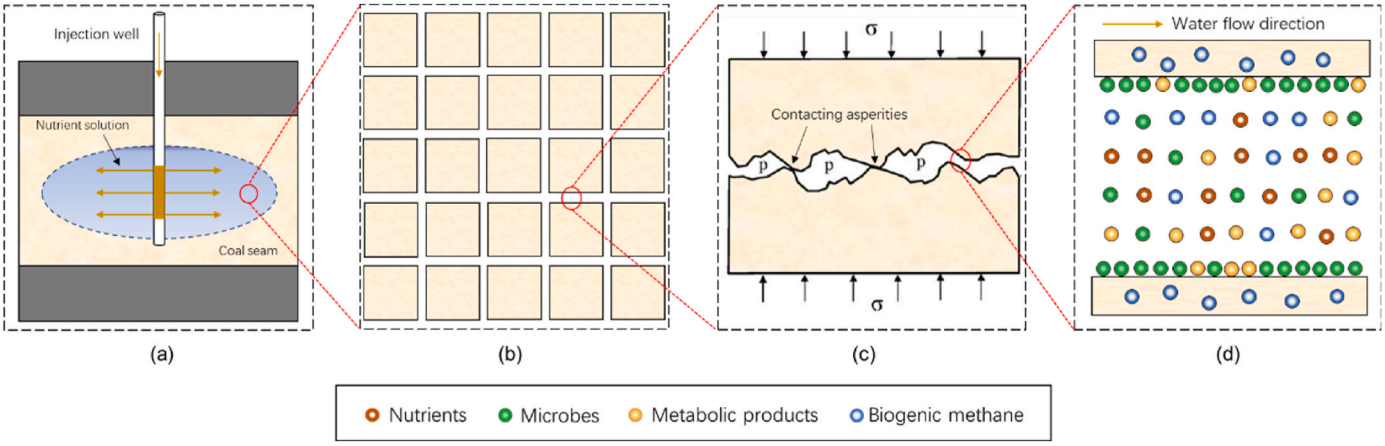

Fig. 1. Mass transport in coal seams during coal-to-gas bioconversion: (a) nutrients solution injection into coal seams; (b) fracture-matrix network in coal seams; (c) a rough-walled fracture under stress-controlled condition; (d) multispecies reactive transport in fracture. Note that σ denotes compressive stress applied to coal and p denotes pore pressure in fracture in this figure.

processes, which implies that one physical process affects the initiation and progress of another (Li et al., 2011). Each individual process has already formed the basis of very well-known disciplines such as hydrology, elasticity, chemistry and biology. The introduction of cross-coupling relations among these processes is the key to more realistically formulate the mathematical model to describe coal bioconversion.

3.1. Geomechanical deformation of coal

All equations in this subsection are derived after the traditional conventions: A comma followed by subscripts represents the differentiation with respect to spatial coordinates, and repeated indices in the same equation imply summation over the range of the indices (Zhang et al., 2008).

The stress equilibrium equation neglecting the inertial term is expressed in the form of:

$$\sigma_{ij,j} + f_i = 0 \tag{1}$$

where σ_{ij} is the component of stress tensor, and f_i is the component of body force.

The strain-displacement relationship is defined as:

$$\varepsilon_{ij} = \frac{1}{2}\left(u_{i,j} + u_{j,i}\right) \tag{2}$$

where ε_{ij} is the component of strain tensor, and u_i is the component of displacement.

For coal seams, gas sorption only results in volumetric strain and does not produce any shear strain. Through making the analogy between thermal expansion and matrix swelling, the constitutive equation for deformable coal is given by:

$$\varepsilon_{ij} = \frac{1}{2G}\sigma_{ij} - \left(\frac{1}{6G} - \frac{1}{9K}\right)\sigma_{kk}\delta_{ij} + \frac{\alpha p_f}{3K}\delta_{ij} + \frac{\beta p_m}{3K}\delta_{ij} + \frac{\varepsilon_s}{3}\delta_{ij} \tag{3}$$

where $G = E/2(1+\nu)$, $K = E/3(1-2\nu)$, $\sigma_{kk} = \sigma_{11} + \sigma_{22} + \sigma_{33}$, $\alpha = 1 - K/K_m$, $\beta = 1 - K_m/K_s$. E is elastic modulus, G is shear modulus, K is bulk modulus, δ_{ij} is Kronecker delta, p_f is fracture pressure, p_m is matrix pressure, α and β are Biot coefficients, and ε_s is gas sorption induced strain.

From Eq. (3), one can obtain:

$$\varepsilon_v = -\frac{1}{K}\left(\overline{\sigma} - \alpha p_f - \beta p_m\right) + \varepsilon_s \tag{4}$$

where $\varepsilon_v = \varepsilon_{11} + \varepsilon_{22} + \varepsilon_{33}$, and $\overline{\sigma} = -\sigma_{kk}/3$. ε_v is the volumetric strain of coal, and $\overline{\sigma}$ is the mean compressive stress.

Integrating Eqs. (1)–(3), the Navier-type equation for coal deformation can be derived:

$$Gu_{i,kk} + \frac{G}{1-2\nu}u_{k,ki} - \alpha p_{f,i} - \beta p_{m,i} - K\varepsilon_L\frac{p_L}{(p_b + p_L)^2}p_{b,i} + f_i = 0 \tag{5}$$

where ε_L is Langmuir strain constant, p_L is Langmuir pressure constant, p_b is coal bulk pressure which is defined as $(1-\varnothing_f)p_m + \varnothing_f p_f$, and $\varnothing_f$ is fracture porosity. In the above equation, the two parameters p_f and p_m are linked to fluid flow equations as will be derived in the following subsection. It should be noted that water-gas two-phase flow presents in the fracture during coal bioconversion. Thus, fracture pressure should be treated as the averaged pressure of water and gas (Ma et al., 2017; Li et al., 2022; Tian et al., 2022):

$$p_f = S_w p_{fw} + S_g p_{fg} \tag{6}$$

where S_w and S_g are the water and gas saturations in the fracture, respectively; and p_{fw} and p_{fg} are the water and gas pressures in the fracture, respectively.

3.2. Fluid flow in coal

3.2.1. Water-gas two-phase flow in fracture

The microbial communities that degrade solid coal to methane gas mainly live within the fracture system of coal seams (Ritter et al., 2015). When nutrients solution is injected into formation, microbes in fractures are stimulated to generate biogenic methane. This is a typical two-phase flow and bio-reactive transport system. The mass conservation equation for each phase in fractures is written as:

$$\frac{\partial\left(\varnothing_f S_w \rho_w\right)}{\partial t} = \nabla \bullet \left(\rho_w \bullet \frac{k_f k_{rw}}{\mu_w}\nabla p_{fw}\right) + Q_w \tag{7}$$

$$\frac{\partial\left(\varnothing_f S_g \rho_{gf} + V_{bg} \bullet \left(1 - \varnothing_{f0} - \varnothing_{ns} - \varnothing_s\right) \bullet \rho_c \bullet \rho_{ga}\right)}{\partial t} = \nabla \bullet \left(\rho_{gf} \bullet \frac{k_f k_{rg}}{\mu_g}\nabla p_{fg}\right) - Q_{fm} + Q_g \tag{8}$$

where $\varnothing_f$ is fracture porosity, S_w is water saturation, ρ_w is water density, k_f is fracture permeability, k_{rw} is relative permeability of water, μ_w is water viscosity, p_{fw} is water pressure in fracture, Q_w is the source term of water phase, S_g is gas saturation, ρ_{gf} is gas density in fracture, k_{rg} is relative permeability of gas, μ_g is gas viscosity, p_{fg} is gas pressure in

fracture, Q_{fm} is gas mass transfer from fracture to matrix, and Q_g is the source term of gas phase.

Herein, more explanation about the term $V_{bg} \bullet (1-\varnothing_{f0}-\varnothing_{ns}-\varnothing_s) \bullet \rho_c \bullet \rho_{ga}$ on the left-hand side of Eq. (8) should be given. In this term, V_{bg} represents the volume of biogenic CBM that can be generated per unit mass of coal; $\varnothing_{f0}$ represents the initial fracture porosity; $\varnothing_{ns}$ represents the fraction of coal that cannot be degraded; $\varnothing_s$ represents the fraction of coal that has already been converted into biogenic CBM; $1-\varnothing_{f0}-\varnothing_{ns}-\varnothing_s$ represents the remaining fraction of coal that still can be converted; ρ_c is coal density; and ρ_{ga} is methane gas density at the standard conditions. Therefore, the term $V_{bg} \bullet (1-\varnothing_{f0}-\varnothing_{ns}-\varnothing_s) \bullet \rho_c \bullet \rho_{ga}$ defines the remaining biogenic CBM mass that still can be generated per unit volume of coal. Note that only $\varnothing_s$ is a variable in this term which can be defined in the form of Eq. (46).

When biogenic methane is generated, gas mass transfer from fracture to matrix occurs under the pressure difference between the two systems. The term for gas mass transfer from fracture to matrix is expressed as (Lim and Aziz, 1995):

$$Q_{fm} = a\rho_{gm}\frac{k_m}{\mu_g}(p_{fg}-p_m) \tag{9}$$

where a is the fracture-matrix transfer shape factor, ρ_{gm} is the gas density in coal matrix, and k_m is the permeability of coal matrix.

The total saturation of water and gas phases in fracture should be equal to one:

$$S_w + S_g = 1 \tag{10}$$

Water and gas are immiscible and separated by a well-defined interface in the fractures. Since the cohesion between water molecules is different from that between gas molecules, there exists a pressure difference between the two phases. This pressure difference is called capillary pressure. The magnitude of capillary pressure is equivalent to difference between non-wetting phase pressure and wetting phase pressure:

$$p_c = p_{fg} - p_{fw} \tag{11}$$

where p_c is capillary pressure. Previous studies have found that capillary pressure has a close relationship with the wetting phase saturation. The Brooks and Corey (1966) formulation is used here to represent this relationship:

$$p_c = p_e S_w^{*\,-1/\lambda} \tag{12}$$

where p_e is the entry pressure of the non-wetting phase, S_w^* is the effective saturation of water phase, and λ is a pore size distribution coefficient.

The effective saturations of water and gas phases are defined as below, respectively:

$$S_w^* = \frac{S_w - S_{wi}}{1 - S_{gr} - S_{wi}} \tag{13}$$

$$S_g^* = \frac{S_g - S_{gr}}{1 - S_{gr} - S_{wi}} \tag{14}$$

where S_{wi} is the irreducible water saturation, S_{gr} is the residual gas saturation, and S_g^* is the effective saturation of gas phase.

Then, the relative permeabilities of water and gas can be respectively defined as (Brooks and Corey, 1966):

$$k_{rw} = S_w^{*\,(3+2/\lambda)} \tag{15}$$

$$k_{rg} = S_g^{*2}\left[1-\left(1-S_g^*\right)^{(1+2/\lambda)}\right] \tag{16}$$

3.2.2. Gas flow and sorption in matrix

As fracture pressure is larger than matrix pressure, the generated biogenic methane gradually transfers from fracture into coal matrix. The mass conservation equation for gas flow in coal matrix is written as:

$$\frac{\partial(m_{mg})}{\partial t} + \nabla \bullet \left(\rho_{gm} \bullet \frac{-k_m}{\mu_g}\nabla p_m\right) = Q_{fm} \tag{17}$$

where $m_{mg} = \varnothing_m\rho_{gm} + \rho_{ga}\rho_c\frac{V_L p_m}{p_m+P_L}$ is the gas mass content in coal matrix including both the free phase gas and adsorbed gas, ρ_{ga} is gas density at standard conditions, ρ_c is coal density, and V_L is Langmuir volume constant. Note that micropores in coal matrix are considered inaccessible to water owing to their small pore dimensions (King et al., 1986).

3.3. Multispecies reactive transport in fracture

Bioconversion of coal to methane involves multiple reaction steps, multiple nutrient ingredients, multiple microbes, and multiple metabolic products. It is impractical to develop a kinetic model that incorporates all the elements in the bioconversion processes as parameter estimation for this model would be unfeasible. Thus, it is reasonable to make the simplification that coal bioconversion kinetics is represented by a single-lumped reaction step, a single-lumped nutrient variable, a single-lumped microbial variable, and a single-lumped metabolic product variable. In coal seams, the movement of nutrients, microbes and metabolic products in the aqueous phase is controlled by advective–dispersive transport. The reactive transport equations for these three species are defined as (Kim, 2006; Li et al., 2011):

$$\frac{\partial(\varnothing_f S_w C_n)}{\partial t} = \nabla \bullet (\varnothing_f S_w D_n \nabla C_n) - \nabla \bullet (v_{fw} C_n) + R_n \tag{18}$$

$$\frac{\partial(\varnothing_f S_w C_m)}{\partial t} = \nabla \bullet (\varnothing_f S_w D_m \nabla C_m) - \nabla \bullet (v_{fw} C_m) + R_m \tag{19}$$

$$\frac{\partial(\varnothing_f S_w C_p)}{\partial t} = \nabla \bullet (\varnothing_f S_w D_p \nabla C_p) - \nabla \bullet (v_{fw} C_p) + R_p \tag{20}$$

where C_n, C_m and C_p are the concentrations of nutrients, microbes, and metabolic products, respectively. D_n, D_m and D_p are the hydrodynamic dispersion coefficients of nutrients, microbes, and metabolic products, respectively. The hydrodynamic dispersion coefficient is typically the summation of mechanical dispersion coefficient and effective diffusion coefficient. v_{fw} is the water flow velocity in fracture. R_n, R_m and R_p are respectively the reaction source terms of nutrients, microbes, and metabolic products which are defined as below:

$$R_n = -Y_s(\varnothing_f S_w C_m + \rho_m \varnothing_1 + \rho_m \varnothing_2) \tag{21}$$

$$R_m = -(k_1+k_3)\varnothing_f S_w C_m + k_2\rho_m\varnothing_1 + (g_1-d_1)\varnothing_f S_w C_m \tag{22}$$

$$R_p = \mu_p(\varnothing_f S_w C_m + \rho_m \varnothing_1 + \rho_m \varnothing_2) \tag{23}$$

where Y_s is microbial growth yield coefficient representing the nutrients consumption rate, ρ_m is the density of microbes, $\varnothing_1$ is the volumetric fraction of microbes adsorbed reversibly on the fracture surface, $\varnothing_2$ is the volumetric fraction of microbes adsorbed irreversibly on the fracture surface, k_1 is the reversible microbial adsorption rate on fracture surface, k_2 is the microbial desorption rate on fracture surface, k_3 is the irreversible microbial adsorption rate on fracture surface, g_1 is the microbial growth rate, d_1 is the microbial decay rate, and μ_p is the metabolic product generation rate.

The modified fracture porosity as a result of microbial adsorption on the fracture surface is defined as:

$$\varnothing_f = \varnothing_{f0} - \varnothing_{mc} = \varnothing_{f0} - \varnothing_1 - \varnothing_2 \tag{24}$$

where $\varnothing_{f0}$ is the initial fracture porosity, and $\varnothing_{mc} = \varnothing_1 + \varnothing_2$ is the porosity occupied by the microbes adsorbed on the fracture surface.

The microbial growth rate is defined by the widely used Monod model (Mitchell et al., 2004):

$$g_1 = g_{1\ max}\frac{C_n}{K_{m/s} + C_n} \tag{25}$$

where $g_{1\ max}$ is the maximum microbial growth rate, and $K_{m/s}$ is the half-saturation constant at which concentration the microbial growth rate reaches half of its maximum value.

3.4. Microbial adsorption/desorption and growth/decay on the fracture surface

Studies have revealed that microbial adsorption can result in porosity reduction of porous medium (Jeong et al., 2019). Traditionally, it is assumed that a uniform biofilm is developed on the fracture surface due to biomass accumulation (Li et al., 2011). According to this assumption, microbial adsorption induced fracture porosity change can be attributed to the volumetric fraction of microbes adsorbed on the fracture surface and to the subsequent growth of biofilm (Li et al., 2011). The suspended microbes in the aqueous phase are assumed to make no change to the effective porosity of fracture system. Based on the above two assumptions, the mass conservation equations for microbes adsorbed reversibly and irreversibly on the fracture surface can be respectively defined as (Kim, 2006):

$$\frac{\partial(\rho_m\varnothing_1)}{\partial t} = k_1\varnothing_f S_w C_m - k_2\rho_m\varnothing_1 + g_1\rho_m\varnothing_1 - d_1\rho_m\varnothing_1 \tag{26}$$

$$\frac{\partial(\rho_m\varnothing_2)}{\partial t} = k_3\varnothing_f S_w C_m + g_1\rho_m\varnothing_2 - d_1\rho_m\varnothing_2 \tag{27}$$

From Eqs. (26) and (27), it can be known that microbial activities on the fracture surface involve microbial adsorption/desorption and growth/decay. Microbial adsorption can be further classified into reversible adsorption and irreversible adsorption.

3.5. Formulation of coal porosity and permeability models

In this section, models for describing coal porosity and permeability change are developed. It is generally accepted that coal permeability is predominantly attributed to the fracture system while matrixes have a negligible contribution. Thus, the porosity and permeability models in this paper specifically refer to fracture porosity and permeability models. Considering a naturally fractured coal containing solid volume V_s and fracture volume V_f, we have the bulk volume $V_b = V_s + V_f$ and the porosity $\varnothing_f = V_f/V_b$. According to Eq. (4), the volumetric change of fractured coal under the loading condition of total stress $\overline{\sigma}$, fracture pressure p_f and matrix pressure p_m can be defined in terms of dV_b/V_b and dV_f/V_f, respectively:

$$\frac{dV_b}{V_b} = -\frac{1}{K}\left(d\overline{\sigma} - \alpha dp_f - \beta dp_m\right) + d\varepsilon_s^b \tag{28}$$

$$\frac{dV_f}{V_f} = -\frac{1}{K_f}\left(d\overline{\sigma} - \gamma dp_f\right) - d\varepsilon_{se} + d\varepsilon_s^f \tag{29}$$

where dV_b/V_b is the volumetric strain of coal bulk, dV_f/V_f is the volumetric strain of coal fracture, K_f is the bulk modulus of fracture, $\gamma = 1 - K_f/K_m$ is Biot coefficient, ε_{se} is stress erosion induced fracture compaction strain, and ε_s^b and ε_s^f are gas sorption induced coal bulk strain and fracture strain, respectively.

Further explanation of Eq. (29) is provided here. From this equation, the fracture volume change is jointly influenced by effective stress, stress erosion, and biogenic methane adsorption. Stress erosion occurs at the contact asperities within the fracture and leads to fracture compaction. This process changes the fracture size but its influence on coal bulk size is negligible. Thus, coal bulk volume change is only influenced by effective stress and biogenic methane adsorption, as shown in Eq. (28).

According to the definition of porosity, the following relationships can be obtained (Detournay and Cheng, 1993):

$$\frac{dV_b}{V_b} = \frac{dV_m}{V_m} + \frac{d\varnothing_f}{1 - \varnothing_f} \tag{30}$$

$$\frac{dV_f}{V_f} = \frac{dV_m}{V_m} + \frac{d\varnothing_f}{\varnothing_f\left(1 - \varnothing_f\right)} \tag{31}$$

Solving Eqs. (28)–(31), one can derive:

$$\frac{d\varnothing_f}{\varnothing_f} = \left(\frac{1}{K} - \frac{1}{K_f}\right)\left(d\overline{\sigma} - dp_f\right) - \frac{\beta}{K}dp_m - d\varepsilon_{se} + d\varepsilon_s^f - d\varepsilon_s^b \tag{32}$$

As coal bulk modulus K is commonly several orders of magnitude larger than fracture bulk modulus K_f, it can be assumed that $\frac{1}{K} - \frac{1}{K_f} \approx -\frac{1}{K_f}$. Then, fracture compressibility can be defined as $c_f = \frac{1}{K_f}$.

Next, integrating Eq. (32) yields:

$$\frac{\varnothing_f}{\varnothing_{f0}} = exp\left[-c_f\left(\Delta\overline{\sigma} - \Delta p_f\right) - \frac{\beta}{K}\Delta p_m - \Delta\varepsilon_{se} + \Delta\varepsilon_s^f - \Delta\varepsilon_s^b\right] \tag{33}$$

As $\frac{\beta}{K}\Delta p_m$ is in the order of 10^{-4}, the contribution of this term to porosity change can be neglected. Thus, it is assumed that $\frac{\beta}{K}\Delta p_m \approx 0$. In addition, microbial adsorption on fracture surface results in porosity reduction and coal solubilization on fracture surface leads to porosity increase. Considering these two influencing factors, coal porosity can be finally expressed as:

$$\frac{\varnothing_f}{\varnothing_{f0}} = exp\left[-c_f\left(\Delta\overline{\sigma} - \Delta p_f\right) - \Delta\varepsilon_{se} + \Delta\varepsilon_s^f - \Delta\varepsilon_s^b\right] + \frac{\varnothing_s}{\varnothing_{f0}} - \frac{\varnothing_{mc}}{\varnothing_{f0}} \tag{34}$$

The cubic law is widely used to define the relation between coal porosity and permeability (Cao et al., 2016; Zeng et al., 2023):

$$\frac{k_f}{k_{f0}} = \left\{exp\left[-c_f\left(\Delta\overline{\sigma} - \Delta p_f\right) - \Delta\varepsilon_{se} + \Delta\varepsilon_s^f - \Delta\varepsilon_s^b\right] + \frac{\varnothing_s}{\varnothing_{f0}} - \frac{\varnothing_{mc}}{\varnothing_{f0}}\right\}^3 \tag{35}$$

In this permeability model, $\varnothing_{mc} = \varnothing_1 + \varnothing_2$ can be obtained from Eqs. (26) and (27). In the following, the expressions for ε_{se}, $\varepsilon_s^f - \varepsilon_s^b$, $\varnothing_s$ are derived.

3.5.1. Fracture strain induced by stress erosion at the contacting asperities

A single fracture in coal can be idealized as two rough surfaces held apart by contacting asperities. When compressive stress is applied on coal, the local stress at the contacting asperities is greatly enhanced due to the small contacting area. The stress concentration leads to grain-contact crushing, followed by a gradually decrease in fracture aperture. When the fracture aperture decreases, the contacting area increases and the local stress decreases concomitantly. Stress erosion and the associated fracture compaction ceases when the local stress approaches the critical stress that implies equilibrium (Yasuhara et al., 2006; Liu et al., 2006). The variation of fracture aperture due to stress erosion at the contacting asperities is defined as (Liu et al., 2006):

$$\frac{dh_{se}}{dt} = k_{se}(\sigma_a - \sigma_c)^n \tag{36}$$

where dh_{se} is the change in fracture aperture due to stress erosion, k_{se} is the stress erosion rate at the contacting asperities, σ_a is the effective stress at the contacting asperities, σ_c is the critical stress which defines the stress state when stress erosion ceases, and n is a constant accounting for micro-cracking at the contacting asperities. In this paper, $n = 1$ is assumed.

Dividing Eq. (36) by the initial fracture aperture, one can obtain the

fracture compaction stain rate:

$$\frac{d\varepsilon_{se}}{dt} = \frac{1}{h_0} \bullet k_{se}(\sigma_a - \sigma_c) \tag{37}$$

where $\frac{d\varepsilon_{se}}{dt}$ is the fracture compaction strain rate, and h_0 is the initial fracture aperture. Integrating Eq. (37) with time, one can obtain $\Delta\varepsilon_{se}$.

Under the triaxial compaction condition, the normal forces acting on the external surface of coal should balance that acting on the contacting asperities within fracture:

$$\sigma_a \bullet A_c^l = \sigma_m \bullet A_t^l \tag{38}$$

where A_c^l is the local contact area, A_t^l is the external surface area, σ_m is the effective normal stress acting on the external surface of coal which is defined as:

$$\sigma_m = \frac{\sigma_{11} + \sigma_{22} + \sigma_{33}}{3} - p_f = \sigma_{cp} - p_f \tag{39}$$

where σ_{cp} is confining pressure.

Rearranging Eq. (38), one can obtain the following relationship:

$$\sigma_a = \frac{\sigma_{cp} - p_f}{R_c} \tag{40}$$

where $R_c = A_c^l / A_t^l$ is the contact area ratio.

Stress erosion induced compaction will irreversibly alter the geometry of fracture surface. A relationship between fracture aperture and contact area ratio should be defined to follow this alteration. Yasuhara and Elsworth (2004) proposed a simplified but physically viable equation to define this relationship:

$$h = h_r + (h_0 - h_r) exp(-(R_c - R_{c0}) / a_0) \tag{41}$$

where h is the current fracture aperture, h_r is the residual fracture aperture, h_0 is the initial fracture aperture, R_{c0} is the initial contact area ratio, and a_0 is a constant.

3.5.2. Coal bulk and fracture strains induced by biogenic methane adsorption

During MECBM operations, biogenic methane is generated through microbial degradation of coal. Under the pressure difference between fracture and matrix systems, the generated biogenic methane gradually diffuses into coal matrix. The adsorption of biogenic methane on coal grains induces coal swelling and influences coal permeability. Three adsorption-induced strains are defined in this work including ε_s^b, ε_s^m, and ε_s^f, representing coal bulk strain, matrix strain and fracture strain, respectively. A strain splitting factor $f = \frac{\Delta\varepsilon_s^f}{\Delta\varepsilon_s^b}$ is introduced to relate coal bulk strain and fracture strain (Jiang et al., 2020). Then, one can obtain:

$$\Delta\varepsilon_s^f - \Delta\varepsilon_s^b = (f-1)\Delta\varepsilon_s^b \tag{42}$$

According to the volume balance principle, the change in coal bulk volume should equal to the change in matrix and fracture volume when coal swells (Jiang et al., 2020):

$$V_{b0}\Delta\varepsilon_s^b = V_{m0}\Delta\varepsilon_s^m + V_{f0}\Delta\varepsilon_s^f \tag{43}$$

where V_{b0}, V_{m0} and V_{f0} are the initial coal bulk volume, matrix volume and fracture volume, respectively.

Laboratory tests (Harpalani and Chen, 1995) have shown that Langmuir-type equation can be used to model gas sorption-induced volumetric strain of coal:

$$\varepsilon_s^i = \frac{\varepsilon_{Li} p_i}{p_{Li} + p_i} \tag{44}$$

where the subscript $i = b, m, f$ denotes coal bulk, matrix and fracture, respectively.

Combining Eqs. (43) and (44), the expression of f can be derived:

$$f = \frac{1}{\varnothing_{f0}}\left[1 - (1-\varnothing_{f0})\frac{\varepsilon_{Lm}p_{Lm}(p_m - p_{m0})(p_b + p_{Lb})(p_{b0} + p_{Lb})}{\varepsilon_{Lb}p_{Lb}(p_b - p_{b0})(p_m + p_{Lm})(p_{m0} + p_{Lm})}\right] \tag{45}$$

where $p_b = (1-\varnothing_f)p_m + \varnothing_f p_f$. Substituting Eq. (45) into Eq. (42), one can obtain the expression of $\Delta\varepsilon_s^f - \Delta\varepsilon_s^b$.

3.5.3. Fracture porosity increase induced by coal solubilization

As microbes mainly live within the fracture system, complex organic compounds on the fracture surface will be gradually degraded into water-soluble intermediates under the action of these microbes during coal bioconversion. In this process, fracture porosity gradually increases while coal matrix size gradually decreases. In this work, it is assumed that coal solubilization rate is directly proportional to the amounts of microbes adsorbed on the fracture surface and the specific surface area of coal matrix blocks:

$$\frac{d\varnothing_s}{dt} = k_+ \bullet \frac{\varnothing_{mc}}{\varnothing_{mc} + K_{mc/s}} \bullet (1 - \varnothing_{f0} - \varnothing_s)^{-\frac{1}{3}} \tag{46}$$

where $\frac{d\varnothing_s}{dt}$ is the changing rate of fracture porosity due to coal solubilization, k_+ is the coal solubilization rate constant, and $K_{mc/s}$ is the half-saturation constant for coal solubilization which represents the volumetric fraction of microbes adsorbed on the fracture surface at which coal solubilization rate reaches half of its maximum value. The term $(1 - \varnothing_{f0} - \varnothing_s)^{-\frac{1}{3}}$ represents the effect of specific surface area of coal matrix blocks on coal solubilization rate. The detailed derivation process of this term can be found in Appendix A.

3.6. Initial and boundary conditions

In order to solve the above governing equations, appropriate initial and boundary conditions are required. First, the geometry of the numerical model is given in Fig. 2. Then, initial and boundary conditions are applied to this 2D model.

For initial conditions, the initial rock displacement, the initial water pressure and saturation in fracture, the initial gas pressure in matrix, the initial concentrations of nutrients, microbes and metabolic products in fracture, the initial fracture strain induced by stress erosion, the initial fracture strain induced by coal solubilization, and the initial volumetric fractions of microbes adsorbed on the fracture surface are given:

$$\vec{u}|_{t=0} = 0 \tag{47}$$

$$p_{fw}|_{t=0} = p_{fw,0}, S_w|_{t=0} = S_{w,0} \tag{48}$$

$$p_m|_{t=0} = p_{m,0} \tag{49}$$

$$C_n|_{t=0} = C_{n,0}, C_m|_{t=0} = C_{m,0}, C_p|_{t=0} = 0 \tag{50}$$

$$\varepsilon_{se}|_{t=0} = 0 \tag{51}$$

$$\varepsilon_{cs}|_{t=0} = 0 \tag{52}$$

$$\varnothing_1|_{t=0} = \varnothing_2|_{t=0} = 0 \tag{53}$$

where $\vec{u}$ is the rock displacement vector.

For mechanical boundary conditions, the normal displacements on the right and lower sides are constrained, and confining pressure is applied on the left and upper sides:

$$\vec{n} \bullet \vec{u} = 0 \quad \text{at the rightand lower sides} \tag{54}$$

$$\sigma = \sigma_{cp} \quad \text{at the left and upper sides} \tag{55}$$

where $\vec{n}$ is the unit outward normal vector to the external sides.

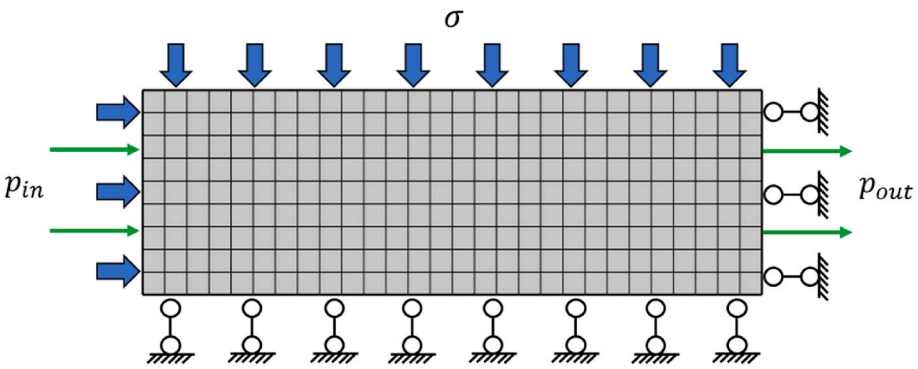

Fig. 2. Geometry of the 2D numerical model.

For flow boundary conditions of the fracture system, the water injection pressure and water saturation are specified on the left side. The water outlet pressure is specified on the right side. Zero water and gas fluxes are specified on both the upper and lower sides:

$$p_{fw} = p_{in} \text{ at the left side} \tag{56}$$

$$S_w = 1 \text{ at the left side} \tag{57}$$

$$p_{fw} = p_{out} \text{ at the right side} \tag{58}$$

$$\vec{n} \bullet \left(\rho_w \bullet -\frac{k_f k_{rw}}{\mu_w}\nabla p_{fw}\right) = \vec{n} \bullet \left(\rho_{gf} \bullet -\frac{k_f k_{rg}}{\mu_g}\nabla p_{fg}\right) = 0 \text{ at the upper and lower sides} \tag{59}$$

For flow boundary conditions of the matrix system, zero gas flow is specified on all of the four external sides:

$$\vec{n} \bullet \left(\rho_{gm} \bullet -\frac{k_m}{\mu_g}\nabla p_m\right) = 0 \text{ at four external sides} \tag{60}$$

For concentration boundary conditions, the injected nutrient concentration and microbial concentration are specified on the left side. Meanwhile, the flux of metabolic product is taken as zero on the left side. On the right side, the concentration gradients of nutrients, microbes, and metabolic products are set as zero. On both the upper and lower sides, zero nutrient, microbe and metabolic product fluxes are specified:

$$C_n = C_{n,i} \text{ at the left side} \tag{61}$$

$$C_m = C_{m,i} \text{ at the left side} \tag{62}$$

$$\vec{n} \bullet \left(-\varnothing_f S_w D_p \nabla C_p + v_{fw} C_p\right) = 0 \text{ at the left side} \tag{63}$$

$$\frac{\partial C_n}{\partial x} = \frac{\partial C_m}{\partial x} = \frac{\partial C_p}{\partial x} = 0 \text{ at the right side} \tag{64}$$

$$\vec{n} \bullet \left(-\varnothing_f S_w D_n \nabla C_n\right) = 0 \text{ at the upper and lower sides} \tag{65}$$

$$\vec{n} \bullet \left(-\varnothing_f S_w D_m \nabla C_m\right) = 0 \text{ at the upper and lower sides} \tag{66}$$

$$\vec{n} \bullet \left(-\varnothing_f S_w D_p \nabla C_p\right) = 0 \text{ at the upper and lower sides} \tag{67}$$

From the above boundary conditions, it can be known that formation water amended nutrients solution is continuously delivered into coal at the left side of the numerical model. Then, the mixture of nutrients, microbes, metabolic products and biogenic methane is extracted from coal at the right side.

4. Model verification

The multiphysics model has been implemented into and solved on the Comsol Multiphysics platform. In this section, the reliability of our model is verified through comparing the numerical simulation results with the laboratory data of biogenic methane generation and coal permeability evolution (Stephen et al., 2014; Lupton et al., 2020). Table 1 summarizes the input parameters for model verification.

4.1. Verification against laboratory data of biogenic methane generation

In the core flooding test by Stephen et al. (2014), subbituminous coal samples collected from the Highvale mine in Alberta were used. Before the test, coal was inoculated with a microbial culture enriched from coal cuttings sampled from a coal seam in Alberta for two weeks. The long incubation period allows the establishment of microbial culture in coal. After the incubation period, coal was continuously flooded with a mineral salt medium and an organic carbon/nitrogen nutrient supplement (tryptone). This nutrient supplement was injected at a flow rate of 0.006 mL/min to feed the microbes in coal. The downstream pressure was set as 3447 kPa. The differential pressure across the coal was gradually increased from 2.027 kPa to 5.136 kPa. The injection of nutrients solution lasts for totally 90 days. Note that no mechanical boundary conditions were applied during the test. Although both CH_4 and CO_2 were generated during the test, only CH_4 was considered in our numerical model. Fig. 3 compares the laboratory data and modelling result of biogenic methane generation. It can be observed that our simulation result has a good agreement with the laboratory data. From this figure, the generation rate of biogenic methane exponentially increases with time. This is because microbial concentration in fracture exponentially increases with time due to the sufficient supply of nutrients during the core flooding test. The input parameters for model verification are summarized in the 2nd column of Table 1. Among these parameters, coal porosity, permeability, and the injected nutrient concentration are provided by Stephen et al. (2014). Other parameters are obtained by matching the experimental data or from the literatures.

4.2. Verification against laboratory data of coal permeability evolution

In the experiments by Lupton et al. (2020), coal samples and formation water used for core flooding were collected from the producing CBM wells in Surat and Bowen Basins. To prepare the nutrients solution, phosphorus and nitrogen were added to the formation water. During the experiments, the fluid injection pressure was maintained at 5 MPa and the confining pressure was maintained at 6 MPa so that an effective stress of 1 MPa was applied on the coal samples. Totally eighteen core flooding experiments were conducted with each group of these experiments lasting for several weeks. As most of the coal permeability curves show the similar trend, three groups of typical coal permeability data are selected to verify our model. In these three groups of laboratory

Table 1
Input parameters for model verification.

Parameter (unit)	Symbols	Value	Value	Value	Value	References
Core no.	–	–	core #1	core #3	core #8	–
Fracture compressibility (MPa^{-1})	c_f	–	0.06	0.04	0.09	–
Elastic modulus (GPa)	E	–	2.7	3	2.5	–
Poisson's ratio	ν	–	0.3	0.3	0.3	–
Initial porosity of matrix	$\varnothing_{m,0}$	–	0.065	0.05	0.08	–
Initial permeability of matrix (m^2)	$k_{m,0}$	–	4.5e-20	1.5e-20	5e-19	–
Initial porosity of fracture	$\varnothing_{f,0}$	0.39	0.024	0.01	0.03	Stephen et al. (2014)
Initial permeability of fracture (m^2)	$k_{f,0}$	13.5e−15	1.5e−17	5e−18	1.6e−16	Stephen et al. (2014), Lupton et al. (2020)
Fracture-matrix transfer shape factor ($1/m^2$)	a	4e6	400	400	400	–
Density of coal (kg/m^3)	ρ_c	1500	1500	1500	1500	Chen et al. (2013)
Methane density at standard conditions (kg/m^3)	ρ_{ga}	0.717	0.717	0.717	0.717	Zhang et al. (2008)
Biogas volume generated per unit mass of coal (m^3/kg)	V_{bg}	0.05	0.05	0.05	0.05	–
Degradable fraction of coal	$\varnothing_s$	0.5	0.5	0.5	0.5	–
Non-degradable fraction of coal	$\varnothing_{ns}$	0.11	0.476	0.49	0.47	–
Initial fracture aperture (mm)	h_0	0.09	0.05	0.05	0.05	–
Residual fracture aperture (mm)	h_r	–	0.007	0.009	0.005	–
Initial contact area ratio	R_{c0}	–	0.02	0.02	0.02	Liu et al. (2006)
Critical stress (MPa)	σ_c	–	11.5	15	10	Liu et al. (2006)
Stress erosion rate (m/MPa/s)	k_{se}	–	3.5e−12	1.5e−12	5e−12	Liu et al. (2006)
Coal solubilization rate constant (m/s)	k_+	2.5e−12	4.5e−12	4.4e−12	4.2e−12	–
Reversible microbial adsorption rate (1/h)	k_1	0.065	0.065	0.065	0.065	Kim (2006), Li et al. (2011)
Microbial desorption rate (1/h)	k_2	0.0012	0.0012	0.0012	0.0012	Kim (2006), Li et al. (2011)
Irreversible microbial adsorption rate (1/h)	k_3	0.01	0.01	0.01	0.01	Kim (2006); Li et al. (2011)
The maximum microbial growth rate (1/h)	$g_{1\ max}$	0.021	0.024	0.024	0.024	Kim (2006), Li et al. (2011)
Microbial decay rate (1/h)	d_1	0.005	0.005	0.005	0.005	Kim (2006), Li et al. (2011)
Microbial density (kg/m^3)	ρ_m	1600	1600	1600	1600	Kim (2006), Li et al. (2011)
Nutrients consumption rate (1/h)	Y_s	1.2e−4	1.8e−4	1.8e−4	1.8e−4	Li et al. (2011)
Metabolic product generation rate (1/h)	μ_p	2.5e−4	3.5e−4	3.5e−4 de	3.5e−4	Li et al. (2011)
Half-saturation constant for coal solubilization (mg/mL)	$K_{mc/s}$	0.001	0.001	0.001	0.001	–
Half-saturation constant for microbial growth (mg/mL)	$K_{m/s}$	20	20	20	20	Chakraborty et al. (2020)
Langmuir strain of coal bulk	ε_{Lb}	0.023	0.02	0.02	0.02	Jiang et al. (2020)
Langmuir pressure of coal bulk (MPa)	p_{Lb}	3.8	4	4	4	Jiang et al. (2020)
Langmuir strain of coal matrix	ε_{Lm}	–	0.025	0.025	0.025	Jiang et al. (2020)
Langmuir pressure of coal matrix (MPa)	p_{Lm}	–	4	4	4	Jiang et al. (2020)
Hydrodynamic dispersion coefficients (m^2/s)	D_n, D_m, D_p	3e−8	1e−8	1e−8	1e−8	Kim (2006), Li et al. (2011)
Initial water saturation	$S_{w,0}$	1	1	1	1	Tian et al. (2022)
Irreducible water saturation	S_{wi}	0.2	0.2	0.2	0.2	Tian et al. (2022)
Residual gas saturation	S_{gr}	0	0	0	0	Tian et al. (2022)
Nonwetting phase entry pressure (MPa)	p_e	0.1	0.1	0.1	0.1	Tian et al. (2022)
Pore size distribution coefficient	λ	2	2	2	2	Tian et al. (2022)
Initial nutrient concentration (mg/mL)	$C_{n,0}$	0.01	0.01	0.01	0.01	–
Initial microbial concentration (mg/mL)	$C_{m,0}$	0.01	0.01	0.01	0.01	–
Initial by-product concentration (mg/mL)	$C_{p,0}$	0	0	0	0	–
Injected nutrient concentration (mg/mL)	$C_{n,i}$	5	0.1	0.094	0.076	–
Injected microbial concentration (mg/mL)	$C_{m,i}$	0	0.01	0.01	0.01	–

experiments, only nutrients injection process was studied. Fig. 4, Figs. 5 and 6 show the comparison between laboratory data and our simulation results. It can be observed that the simulation results have a good agreement with the laboratory data. For core #1, coal permeability rapidly declines within the initial 15 days and then slowly declines till the end of the experiment. For core #3, coal permeability rapidly declines within the initial 30 days and then slowly declines till the end of the experiment. For core # 8, coal permeability rapidly declines within the initial 20 days and then slowly declines till the end of the experiment. The initial rapid permeability decline is due to stress erosion at the contacting asperities within the fracture. The permeability decline magnitude and decline rate are determined by the critical stress that implies equilibrium and stress erosion rate constant, respectively. The later slow decline in permeability is the combined results of coal

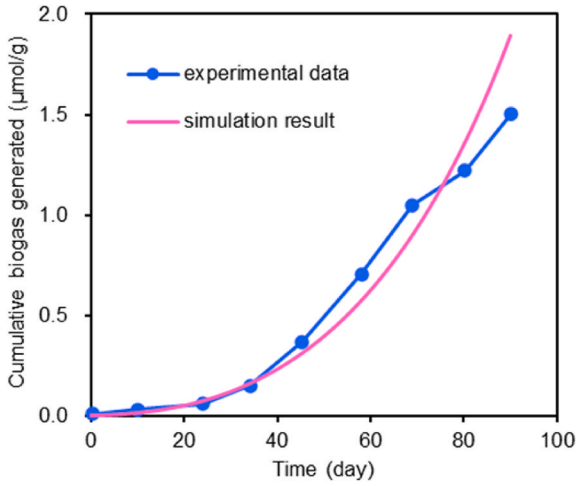

Fig. 3. Comparison between laboratory data and modelling result.

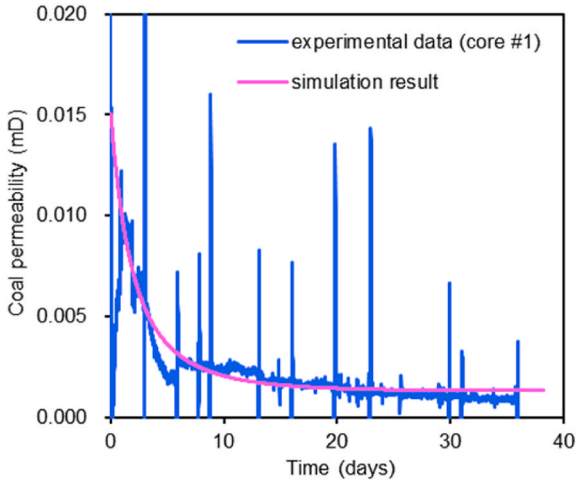

Fig. 4. Comparison between laboratory data (core #1) and simulation result.

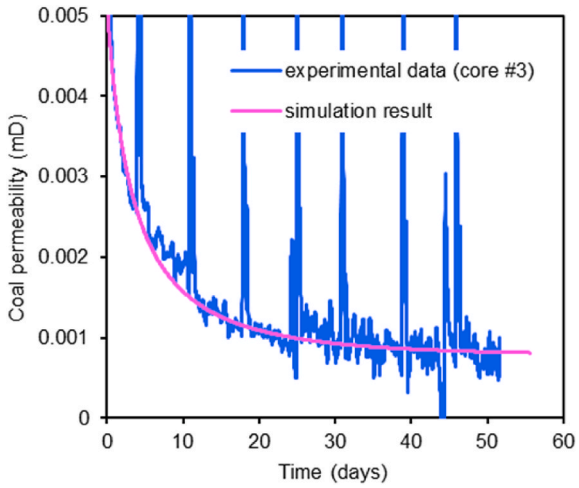

Fig. 5. Comparison between laboratory data (core #3) and simulation result.

solubilization, biogenic methane adsorption on coal matrix, and microbial adsorption on the fracture surface. Due to the low concentration of injected nutrients, coal solubilization rate is very slow and thus no obvious rebound in coal permeability can be observed. Meanwhile, the

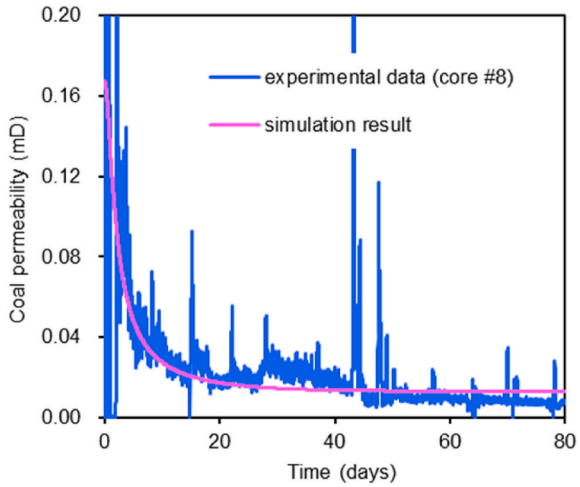

Fig. 6. Comparison between laboratory data (core #8) and simulation result.

growth rate of microbes and the adsorbed amount of biogenic methane are also very low which explains why coal permeability slowly declines in the later stage. The input parameters for model verification are summarized in the 3rd, 4th and 5th columns of Table 1. The mechanical loading parameters and injected nutrient concentration are provided by Lupton et al. (2020). Other geomechanical and physical parameters are obtained by matching the experimental data or from the literatures. It should be mentioned here that the modelled permeability curves represent the permeability evolution behavior at the center point of the numerical model.

5. Results and analysis

The proposed multiphysics model can provide new insights into the interactions of multiple processes during coal-to-methane bioconversion. In this section, the involved important processes are analyzed. For the parametric studies, the impacts of injected nutrient concentration, injected microbial concentration, microbial growth rate, initial coal permeability and degradable fraction of coal on biogenic methane generation and extraction are investigated. In each parametric study group, only one input parameter is changed with all the other parameters keeping identical to that of the base case. As shown in Table 2, we simulate totally six cases. In all these cases, coal is under the constant confining pressure condition. The initial pressure of coal is 1 MPa, the injection pressure is 4 MPa, and the confining pressure is 7 MPa.

Table 2
Simulation strategies.

Cases	$C_{n,i}$ (mg/mL)	$C_{b,i}$ (mg/mL)	$g_{1\ max}$ (1/h)	k_{f0} (m^2)	$\varnothing_{s\_max}$
Base case	5.0	0.05	0.024	1e-16	0.5
Case 1	4.8/5.0/5.2	0.05	0.024	1e-16	0.5
Case 2	5.0	0.03/0.05/0.07	0.024	1e-16	0.5
Case 3	5.0	0.05	0.023/0.024/0.025	1e-16	0.5
Case 4	5.0	0.05	0.024	1e-17/1e-16/1e-15	0.5
Case 5	5.0	0.05	0.024	1e-16	0.4/0.5/0.6

$C_{n,i}$ represents the injected nutrient concentration.
$C_{b,i}$ represents the injected microbial concentration.
$g_{1\ max}$ represents the maximum microbial growth rate.
k_{f0} represents the initial coal permeability.
$\varnothing_{s\_max}$ represents the fraction of coal that can be degraded into methane gas.

Excluding the nutrient concentration, microbial concentration, microbial growth rate, initial coal permeability, degradable fraction of coal and the mechanical loading conditions, all the other input parameters for numerical simulation are identical to that in the last column of Table 1. In this work, the size of the numerical model is set as 30 cm*100 cm, and the nutrients are injected until the degradable fraction of coal is completely degraded.

5.1. Base case results

5.1.1. Evolution of nutrient concentration in the aqueous phase

In the initial state, coal sample contains low concentration (0.05 mg/mL) of nutrients. During nutrients injection process, a constant nutrient concentration of 5 mg/mL is applied at the inlet. Fig. 7 shows the dynamic variation of nutrient concentration throughout coal during bioconversion. As can be seen, the nutrient concentration increases with time before the 25th hour. After the 25th hour, the nutrient concentration remains unchanged.

5.1.2. Evolution of microbial concentration in the fracture system

In the initial state, coal sample contains low concentration (0.05 mg/mL) of microbes. As nutrients are injected into coal seams using formation water (Ritter et al., 2015) which usually contains low concentration of microbes, a constant microbial concentration of 0.05 mg/mL is applied at the inlet. Fig. 8 shows the dynamic variation of microbial concentration in the aqueous phase throughout coal. As can be seen, microbial concentration decreases before the 20th hour. This is because deposition of microbes from the aqueous phase to the fracture surface controlling microbial concentration in this period of time. From the 20th hour to the 1900th day, microbial concentration gradually increases as continuous supply of microbes from the inlet, microbial growth in the aqueous phase, and microbial desorption from the fracture surface gradually outcompete the effect of microbial deposition. After the 1900th day, microbial concentration in the aqueous phase remains unchanged as a result of continuous supply of microbes from the inlet at a constant concentration.

In the initial state, we assume that there are no microbes adsorbed on the fracture surface. During nutrients solution injection, microbes from aqueous phase deposit and adsorb to the fracture surface at a constant rate. Meanwhile, these adsorbed microbes continue to grow at a constant rate. These two processes explain why microbial concentration on the fracture surface exponentially increase during coal bioconversion, as can be seen from Fig. 9.

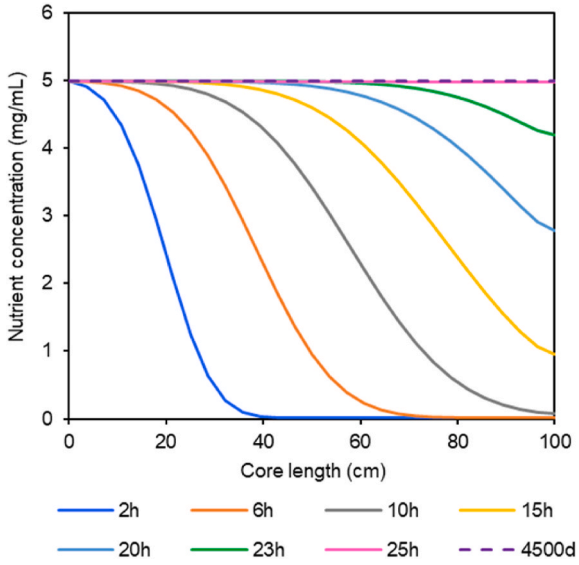

Fig. 7. Dynamic variation of nutrient concentration throughout coal.

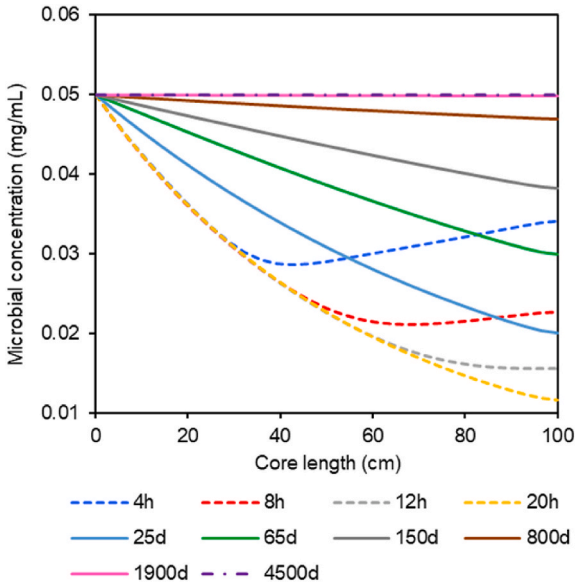

Fig. 8. Dynamic variation of microbial concentration in the aqueous phase.

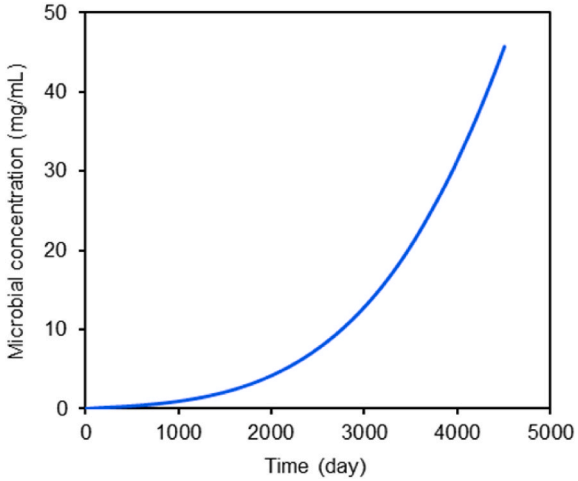

Fig. 9. Dynamic variation of microbial concentration $(\varnothing_1 + \varnothing_2) \bullet \rho_m$ on the fracture surface.

5.1.3. Evolution of metabolic product concentration in the aqueous phase

In the initial state, coal sample contains no metabolic products. During nutrients injection, metabolic products are gradually generated through microbial degradation of coal. Fig. 10 shows the dynamic variation of metabolic product concentration in the aqueous phase throughout coal. As can be seen, metabolic product concentration gradually increases within the initial 275 days. This is because coal permeability is relatively low within this period of time and thus the generated metabolic products gradually accumulate within the fracture system. However, after the 275th day, metabolic product concentration starts to decrease. This is because coal permeability exponentially increases in this process (see Fig. 12) and thereby these generated metabolic products flow out of coal at a faster rate than before. It can also be observed that metabolic product concentration gradually increases from the inlet to the outlet as the generated metabolic products accumulate and flow out of coal sample at the outlet.

5.1.4. Evolution of biogenic methane saturation in the fracture system

In the initial state, fracture system is fully saturated with water. During nutrients injection, a constant water saturation of 1 is applied at

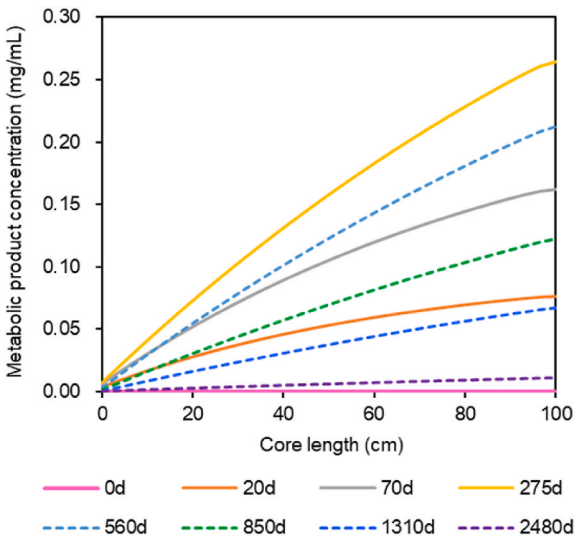

Fig. 10. Dynamic variation of metabolic product concentration throughout coal.

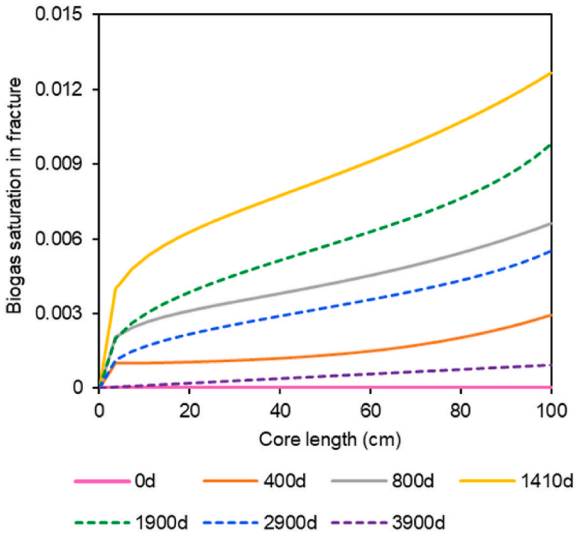

Fig. 11. Dynamic variation of biogenic gas saturation throughout coal.

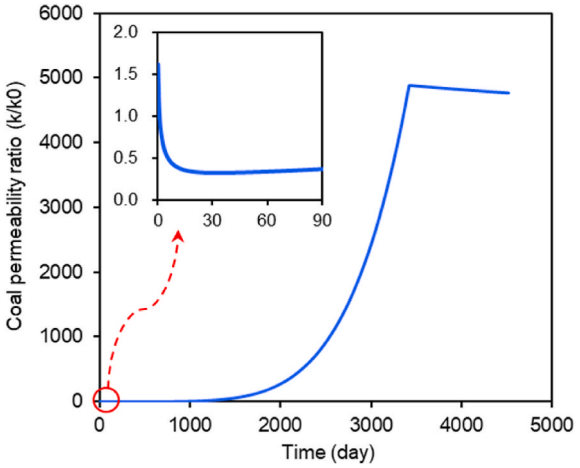

Fig. 12. Long-term evolution behavior of coal permeability.

the inlet. Biogenic methane is then gradually generated through microbial degradation of coal. Fig. 11 shows the dynamic variation of gas saturation throughout coal during bioconversion. As can be seen, gas saturation in coal initially increases and then decreases. Similar to metabolic product concentration variation, the variation of gas saturation in coal is also controlled by coal permeability variation. It can also be observed that gas saturation gradually increases from inlet to outlet. This is because the generated biogenic methane accumulates and flows out of coal at the outlet.

5.1.5. *Evolution of coal permeability*

Eq. (35) is used to model coal permeability evolution during bioconversion. This equation considers the impacts of effective stress, stress erosion, coal solubilization, biogenic methane adsorption, and microbial adsorption on coal permeability change. Fig. 12 shows the long-term evolution behavior of coal permeability. Within the initial 90 days, coal permeability first increases due to nutrients solution injection. Then, coal permeability declines at a relatively large rate as a result of stress erosion at the contacting asperities. After that, coal permeability slowly increases under the joint impacts of coal solubilization, biogenic methane adsorption, and microbial adsorption. Although biogenic methane adsorption on coal matrix and microbial adsorption on fracture surface lead to coal permeability decline in this process, coal solubilization induced permeability rebound is more pronounced. After the 90th day, coal permeability constantly increases owing to coal solubilization until the degradable fraction of coal is completely degraded at the 3430 days. After that, coal bioconversion ceases and coal permeability declines purely due to microbial adsorption and growth on the fracture surface.

5.1.6. *Biogenic methane generation and extraction*

Fig. 13 shows the cumulative biogenic methane converted from coal and the amount of biogenic methane extracted. For the cumulative biogenic methane generation curve, it first exponentially increases and then stabilizes. The modelled biogenic methane generation behavior in the initial 90 days has been confirmed in some laboratory core flooding tests (Stephen et al., 2014; Lupton et al., 2020). Here, it should be mentioned again that biogenic methane generation is influenced by many factors. The more-reliable simulations still require more-realistic input parameters which should be derived from well-designed new experiments. For further observation, the extracted biogenic methane is less than the generated biogenic methane because part of the generated biogenic methane diffuses into coal matrix and adsorbs on coal grains under the pressure difference between fracture and matrix systems.

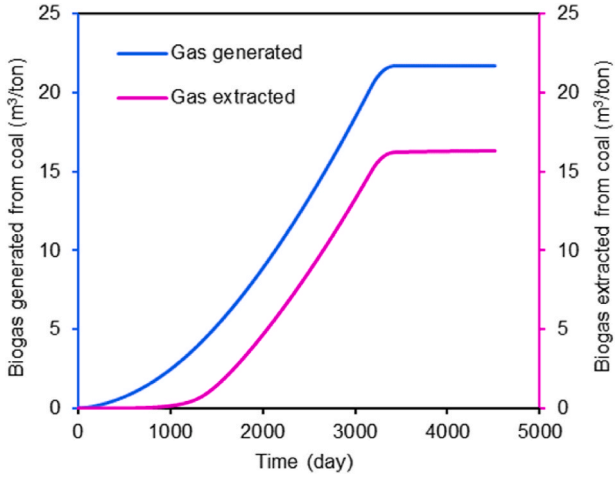

Fig. 13. Cumulative biogenic methane generated and extracted from coal. Note that the unit "m^3/ton" in this figure denotes standard cubic meter of biogenic methane generated per ton of coal.

5.2. Parametric studies

5.2.1. Case 1: influence of injected nutrient concentration

In this subsection, we investigate the impact of injected nutrient concentration on biogenic methane generation and extraction. From Fig. 14, biogenic methane is generated and extracted at a faster rate when injected nutrient concentration increases from 4.8 to 5.2 mg/mL. The primary reason for this effect is that microbes grow faster in the higher nutrient concentration environment, thereby decomposing coal and generating biogenic methane at a faster rate. It can also be found that the total amount of the generated and extracted biogenic methane remains the same for all cases. This is mainly because the degradable fraction of coal and the Langmuir parameters are set as the same for all cases.

5.2.2. Case 2: influence of injected microbial concentration

In this subsection, we investigate the impact of injected microbial concentration on biogenic methane generation and extraction because the injected formation water usually contains a certain number of indigenous microbes. From Fig. 15, biogenic methane is generated and extracted at a faster rate when the injected microbial concentration increases from 0.03 to 0.07 mg/mL. This is because coal solubilization rate is directly proportional to the microbial population on the fracture surface. The larger the injected microbial concentration is, the more the microbes adsorb on the fracture surface. It can also be found that the total amount of the generated and extracted biogenic methane remains the same for all cases.

5.2.3. Case 3: influence of microbial growth rate

In this subsection, we vary the maximum microbial growth rate from 0.023 to 0.025 1/h to investigate the impact of microbial growth on biogenic methane generation and extraction. From Fig. 16, biogenic methane is generated and extracted at a faster rate when microbial growth rate increases. This is because faster microbial growth leads to larger microbial population on the fracture surface and then results in faster coal-to-methane bioconversion. In addition, it can be found that the total amount of the generated and extracted biogenic methane remains the same for all cases.

5.2.4. Case 4: influence of initial coal permeability

In this subsection, we investigate the impact of initial coal permeability on biogenic methane generation and extraction. From Eqs. (26) and (27), a major portion of microbes live on the fracture surface are deposited from the injected formation water. As a larger coal permeability is favorable for delivering more formation water through the coal, more microbes deposit on the fracture surface when coal permeability increases from 0.01 mD to 1 mD, which results in faster coal solubilization and biogenic methane generation and extraction, see Fig. 17. In addition, it can be found that the total amount of the generated and extracted biogenic methane remains the same for all cases.

5.2.5. Case 5: influence of degradable fraction of coal

The degradable fraction of coal represents the fraction of coal that can be converted into biogenic gas during bioconversion. In this subsection, we investigate the impact of the degradable fraction of coal on biogenic methane generation and extraction. From Fig. 18, more time is required to generate and extract more biogenic methane from coal when degradable fraction of coal increases from 0.4 to 0.6, but the generation rate and extraction rate remain the same for all the cases as microbe related parameters are kept unchanged.

6. Conclusions

In this work, a multiphysics model has been developed for quantifying coal-to-methane bioconversion and extraction processes. These processes include (1) coal deformation; (2) water and gas flow; (3) multispecies reactive transport; and (4) microbial growth/decay and adsorption/desorption. All these processes are coupled through coal porosity and permeability model that links hydrological, mechanical, chemical and biological processes together. The validity of this multiphysics model is verified through comparing the modelling results with laboratory coal bioconversion data. Applying this multiphysics model, the practical operation is simulated in which nutrients solution is continuously delivered into coal seams. Based on our modelling results, the following conclusions can be drawn:

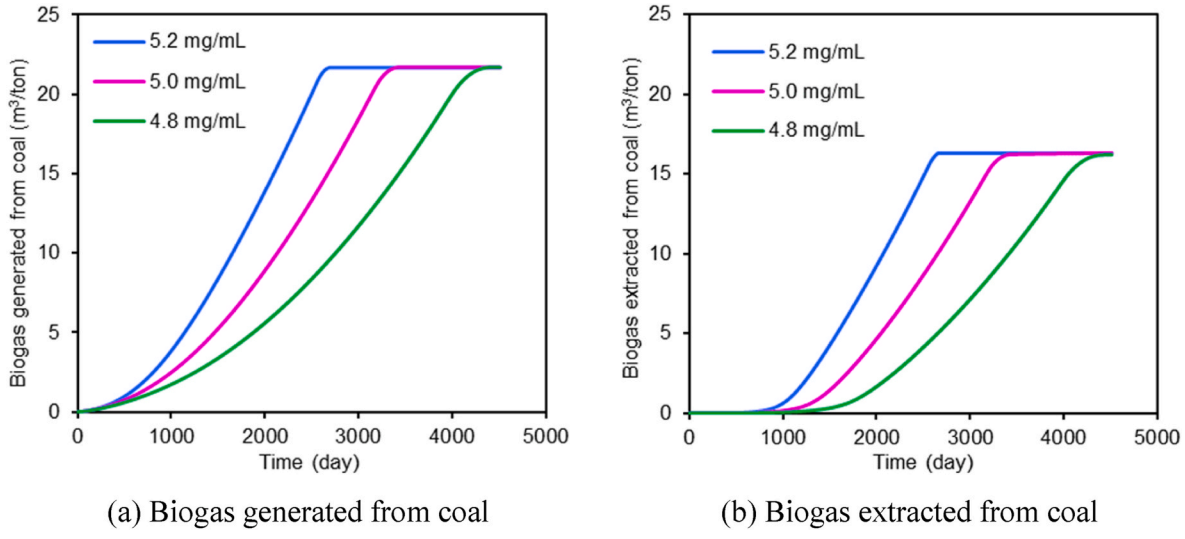

Fig. 14. Impact of injected nutrient concentration on biogenic methane generation and extraction.

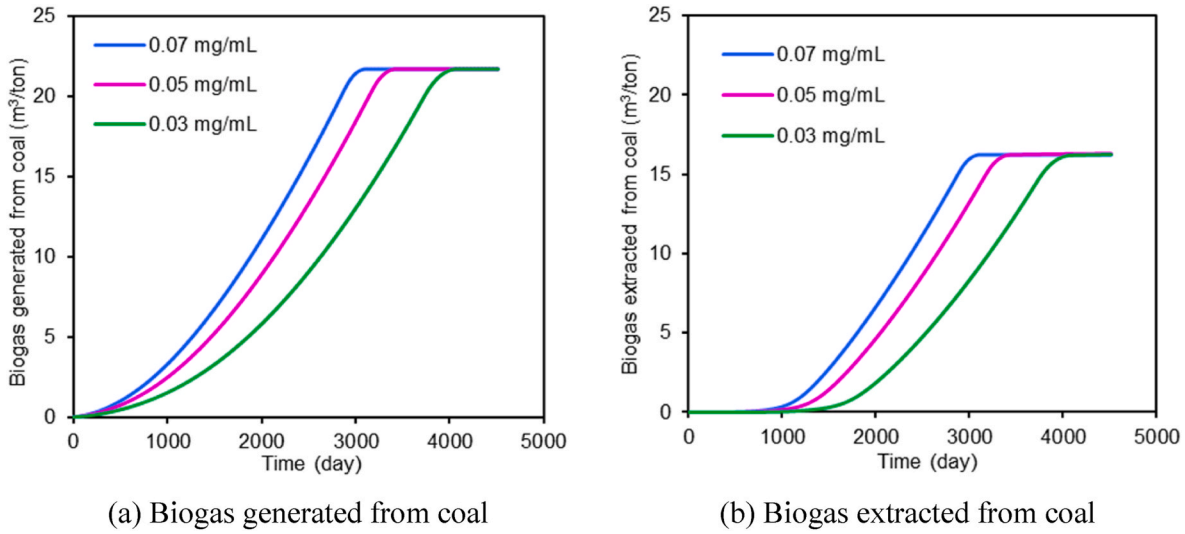

Fig. 15. Impact of injected microbial concentration on biogenic methane generation and extraction.

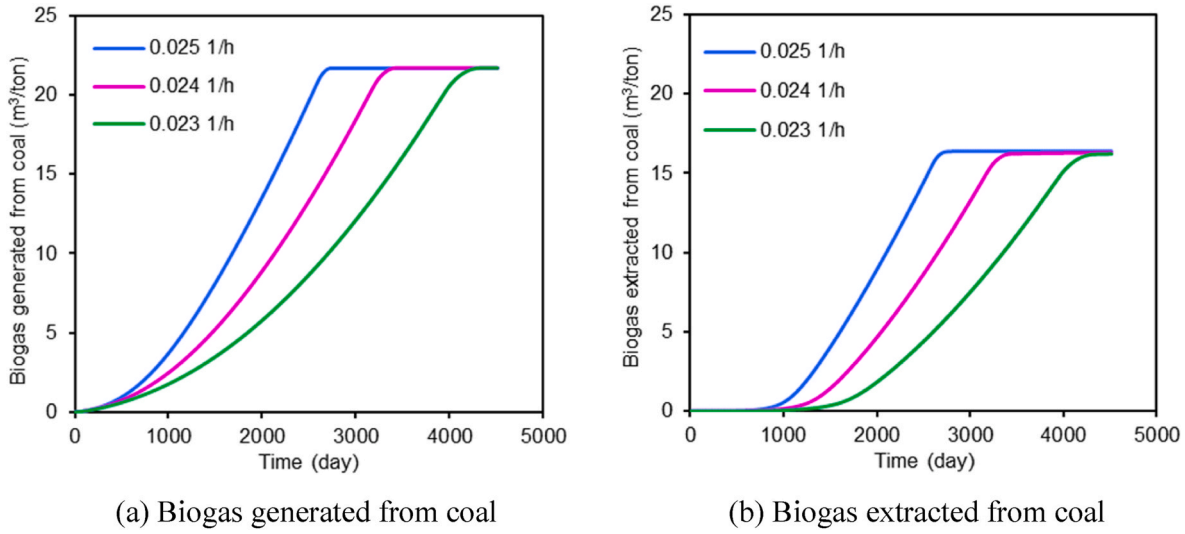

Fig. 16. Impact of microbial growth rate on biogenic methane generation and extraction.

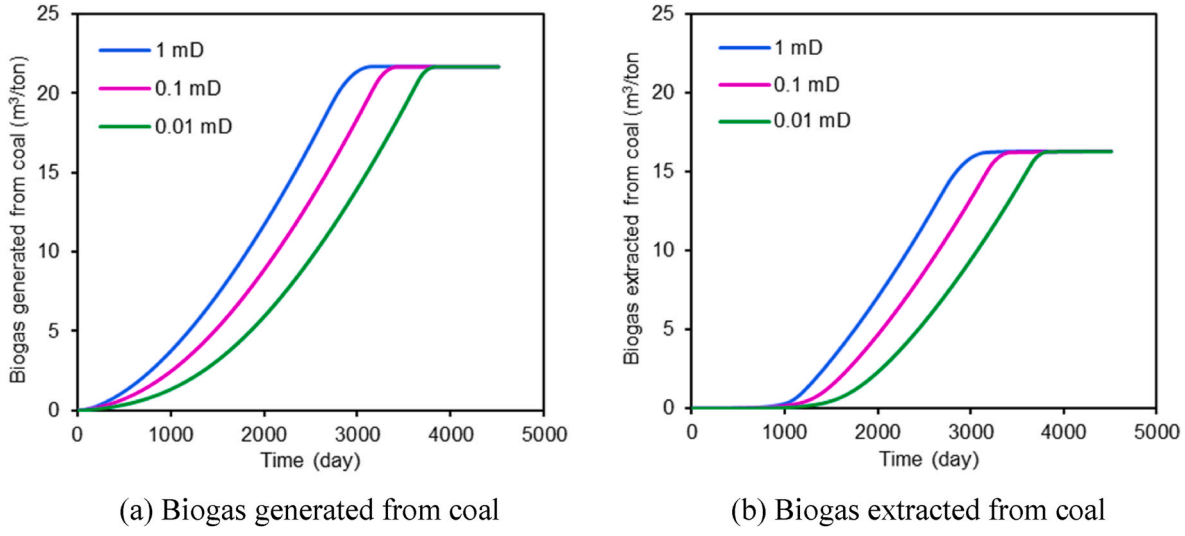

Fig. 17. Impact of initial coal permeability on biogenic methane generation and extraction.

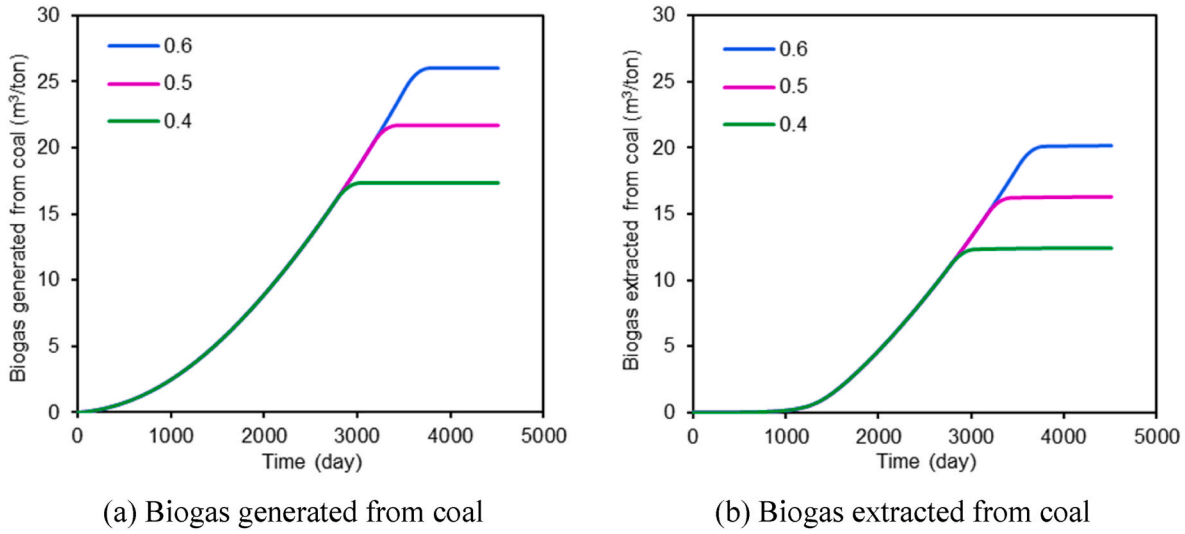

Fig. 18. Impact of degradable fraction of coal on biogenic methane generation and extraction.

(1) The total amount of biogenic gas that can be generated is controlled by the fraction of coal that can be converted while biogenic gas generation and extraction rates are controlled by nutrient concentration, microbial concentration, microbial growth rate and initial coal permeability. All positive relations can be observed.
(2) Not all generated biogenic gas can be extracted. When coal-to-methane bioconversion occurs, part of the generated biogenic gas diffuses into coal matrix and adsorbs on coal grains under the pressure difference between fracture and matrix systems. Thus, only the remaining free phase biogenic gas in the fracture system can be extracted from coal.
(3) The impact of initial coal permeability on biogenic gas generation and extraction is significant. If initial permeability of coal seam is low, stimulation treatments like hydraulic fracturing are necessary as artificially created fracture networks can provide more permeable pathways for nutrients delivery, physically increase microbial access to coal, decrease the specific surface area of coal matrix blocks and, thus, improve coal-to-gas bioconversion rate.
(4) The evolution of coal permeability during bioconversion is also significant. Nutrients injection and coal solubilization play the key role for increasing coal permeability while stress erosion, biogenic methane adsorption and microbial adsorption lead to coal permeability decline. Under the joint impacts of these influencing factors, coal permeability initially declines and then rebounds and constantly increases until coal bioconversion ceases.

Declaration of competing interest

The authors declare that they have no known competing financial interests or personal relationships that could have appeared to influence the work reported in this paper.

Data availability

Data will be made available on request.

Acknowledgements

This work is supported by the Australian Research Council under Grant DP200101293. The first author is also supported by the UWA-China Joint Scholarships (Grant No. 201906450050). These supports are gratefully acknowledged.

Appendix A

In this work, we use the cubic model to represent the microstructure of coal. In this arrangement, coal matrix blocks are surrounded by orthogonal fractures. During coal-to-gas bioconversion, the size of coal matrix block gradually decreases, as shown in Fig. A1. The decrease of coal matrix block size will induce the change of the specific surface area of coal matrix block, thereby influencing coal solubilization rate. With the assumption that coal solubilizes at the same rate on all surfaces of a single matrix block, the specific surface area of a single matrix block can then be defined as:

$$S=\frac{6\left[L_0{}^3\left(1-\varnothing_{f0}-\varnothing_s\right)\right]^{\frac{2}{3}}}{L_0{}^3\left(1-\varnothing_{f0}-\varnothing_s\right)}=\frac{6}{L_0}\left(1-\varnothing_{f0}-\varnothing_s\right)^{-\frac{1}{3}} \tag{A1}$$

where L_0 represents the sum of the initial coal matrix width and the initial fracture aperture.

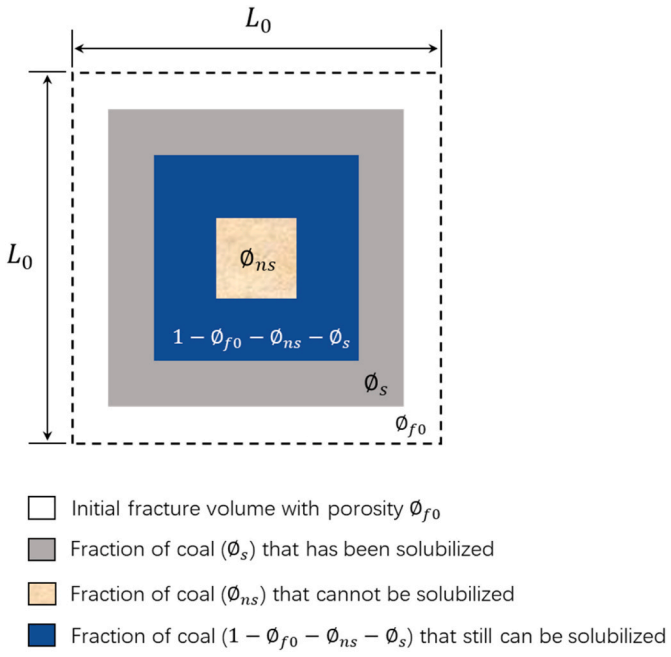

Fig. A1. The evolution of coal structure during bioconversion.

References

Brooks, R.H., Corey, A.T., 1966. Properties of porous media affecting fluid flow. J. Irrigat. Drain. Div. 92 (2).

Cao, P., et al., 2016. General gas permeability model for porous media: bridging the gaps between conventional and unconventional natural gas reservoirs. Energy Fuels 30 (7), 5492–5505.

Chakraborty, S., et al., 2020. Numerical modeling on the influence of effective porosity, microbial kinetics, and operational parameters on enhanced oil recovery by microbial flooding within a sandstone formation. SPE J. 25 (6), 2932–2961.

Chen, Z.W., et al., 2013. Roles of coal heterogeneity on evolution of coal permeability under unconstrained boundary conditions. J. Nat. Gas Sci. Eng. 15, 38–52.

Detournay, E., Cheng, A.H.-D., 1993. Fundamentals of poroelasticity. In: Fairhurst, C. (Ed.), Chapter 5 in Comprehensive Rock Engineering: Principles, Practice and Projects, vol. 2. Pergamon Press, pp. 113–171.

Emmert, S., et al., 2020. Importance of specific substrate utilization by microbes in microbially enhanced coal-bed methane production: a modelling study. Int. J. Coal Geol. 229, 103567.

Gupta, P., Gupta, A., 2014. Biogas production from coal via anaerobic fermentation. Fuel 118, 238–242.

Harpalani, S., Chen, G., 1995. Estimation of changes in fracture porosity of coal with gas emission. Fuel 74, 1491–1498.

Jeong, M.S., et al., 2019. Critical review on the numerical modeling of in-situ microbial enhanced oil recovery processes. Biochem. Eng. J. 150, 107294.

Jiang, C.Z., et al., 2020. Controlling effects of differential swelling index on evolution of coal permeability. J. Rock Mech. Geotech. Eng. 12, 461–472.

Jones, E.J., et al., 2010. Stimulation of methane generation from nonproductive coal by addition of nutrients or a microbial consortium. Appl. Environ. Microbiol. 76, 7013–7022.

Kim, S.B., 2006. Numerical analysis of bacterial transport in saturated porous media. Hydrol. Process. 20, 1177–1186.

King, G.R., et al., 1986. Numerical simulation of the transient behavior of coal-seam degasification wells. SPE Form. Eval. 1 (2), 165–183.

Li, J., et al., 2011. Interactions of microbial-enhanced oil recovery processes. Transport Porous Media 87, 77–104.

Li, W., et al., 2022. Water liberating/sealing effects on shale gas extraction: a fully coupled multidomain and multiphysics model. Fuel 325, 124953.

Lim, K.T., Aziz, K., 1995. Matrix-fracture transfer shape factors for dual-porosity simulators. J. Petrol. Sci. Eng. 13, 169–178.

Liu, J.S., et al., 2006. A fully-coupled hydrological-mechanical-chemical model for fracture sealing and preferential opening. Int. J. Rock Mech. Min. Sci. 43, 23–36.

Lupton, N., et al., 2020. Enhancing biogenic methane generation in coalbed methane reservoirs –Core flooding experiments on coals at in-situ conditions. Int. J. Coal Geol. 219, 103377.

Ma, T., et al., 2017. Fully coupled two-phase flow and poromechanics modeling of coalbed methane recovery: impact of geomechanics on production rate. J. Nat. Gas Sci. Eng. 45, 474–486.

Meslé, M., et al., 2016. Design of a small-scale high-pressure reactor system to study microbial bioconversion of coal to methane. In: Geologic Energy Research, Presented at the GSA Annual Meeting, Denver, Colorado, U.S.A.

Mitchell, D.A., et al., 2004. A review of recent developments in modeling of microbial growth kinetics and intraparticle phenomena in solid-state fermentation. Biochem. Eng. J. 17, 15–26.

Opara, A., et al., 2012. Microbial production of methane and carbon dioxide from lignite, bituminous coal, and coal waste materials. Int. J. Coal Geol. 96, 1–8.

Pandey, R., et al., 2016. Changes in gas storage and transport properties of coal as a result of enhanced microbial methane generation. Fuel 179, 114–123.

Pandey, R., Harpalani, S., 2019a. Evaluation of dynamic flow and production behavior of biogenic methane reservoirs. In: Presented at the 53rd US Rock Mechanics/ Geomechanics Symposium Held in New York, NY, USA.

Pandey, R., Harpalani, S., 2019b. Impact of bioconversion on matrix strain response of coal reservoirs: Part 1-Experimental insights. Fuel 239, 1363–1375.

Park, S.Y., Liang, Y.N., 2016. Biogenic methane production from coal: a review on recent research and development on microbially enhanced coalbed methane (MECBM). Fuel 166, 258–267.

Rice, D.D., Claypool, G., 1981. Generation, accumulation, and resource potential of biogenic gas. AAPG Bull. 65.

Ritter, D., et al., 2015. Enhanced microbial coalbed methane generation: a review of research, commercial activity, and remaining challenges. Int. J. Coal Geol. 146, 28–41.

Saurabh, S., Harpalani, S., 2018. Modeling of microbial methane generation from coal and assessment of its impact on flow behavior. Fuel 216, 274–283.

Scott, A.R., 1995. Limitations and possible benefits of microbially enhanced coalbed methane. In: Presented at the International Unconventional Gas Symposium. University of Alabama, Tuscaloosa, pp. 423–432.

Scott, A.R., 1999. Improving coal gas recovery with microbially enhanced coalbed methane. In: Coalbed Methane: Scientific, Environmental and Economic Evaluation. Springer, pp. 89–110.

Senthamaraikkannan, G., et al., 2016a. Kinetic modeling of the biogenic production of coalbed methane. Energy Fuels 30, 871–883.

Senthamaraikkannan, G., et al., 2016b. Development of a multiscale microbial kinetics coupled gas transport model for the simulation of biogenic coalbed methane production. Fuel 167, 188–198.

Senthamaraikkannan, G., et al., 2016c. Multiphase reactive-transport simulations for estimation and robust optimization of the field scale production of microbially enhanced coalbed methane. Chem. Eng. Sci. 149, 63–77.

Sharma, A., et al., 2018. Modeling framework for biogenic methane formation from coal. Energy Fuels 32, 8453–8461.

Stephen, A., et al., 2014. Bioconversion of coal: new insights from a core flooding study. RSC Adv. 4, 22779–22791.

Strapoc, D., et al., 2008. Methane-producing microbial community in a coal bed of the Illinois Basin. Appl. Environ. Microbiol. 74, 2424–2432.

Strapoc, D., et al., 2011. Biogeochemistry of microbial coal-bed methane. Annu. Rev. Earth Planet Sci. 39, 617–656.

Su, X.B., et al., 2022. Experimental study of advantages of coalbed gas bioengineering. J. Nat. Gas Sci. Eng. 102, 104585.

Tian, J.W., et al., 2022. Linking fractal theory to a fully coupled coal deformation and two-phase flow multiphysics: the role of fractal dimensions. Energy Fuels 36 (20), 12591–12605.
Yasuhara, H., Elsworth, D., 2004. The evolution of permeability in a natural fracture: the significant role of pressure solution. J. Geophys. Res. 109, B03204.
Yasuhara, H., et al., 2006. Spontaneous switching between permeability enhancement and degradation in fractures in carbonate: lumped parameter representation of mechanically- and chemically-mediated dissolution. Transport Porous Media 65, 385–409.
Zeng, J., et al., 2023. Anisotropic permeability model for coal considering stress sensitivity, matrix anisotropic internal swelling/shrinkage, and gas rarefaction effects. Energy Fuels 37 (4), 2811–2832.
Zhang, H.B., et al., 2008. How sorption-induced matrix deformation affects gas flow in coal seams: a new FE model. Int. J. Rock Mech. Min. Sci. 45, 1226–1236.
Zhang, J., et al., 2016a. Finding cost-effective nutrient solutions and evaluating environmental conditions for biogasifying bituminous coal to methane ex situ. Appl. Energy 165, 559–568.
Zhang, J., et al., 2016b. Optimization of methane production from bituminous coal through biogasification. Appl. Energy 183, 31–42.
Zhang, R., et al., 2017. Changes in pore structure of coal caused by coal-to-gas bioconversion. Sci. Rep. 7, 3840.
Zhi, S., et al., 2018. Hydraulic fracturing for improved nutrient delivery in microbially-enhanced coalbed-methane (MECBM) production. J. Nat. Gas Sci. Eng. 60, 294–311.